Multiple Attribute Group Decision-Making with Neutrosophic Environment for Carbon Emission Prediction on Sustainable Urban Management

Mesfer Al Duhayyim[*1]

[1]Department of Computer Science, College of Computer Engineering and Sciences, Prince Sattam bin Abdulaziz University, Al-Kharj 16273, Saudi Arabia
Emails: m.alduhayyim@psau.edu.sa

Abstract

Sufficient CO2 is indispensable for vegetation, but space and oceanic vehicles, industrial chimneys and land use tons of extreme CO2 and are typically accountable for global warming, climate variations and greenhouse effect. Owing to COVID19, CO2 discharge was in 2020 at its lower level than first ten years. However, the time taken is not known to decrease, increase or change carbon emissions to an endurable point. Precise predicting of carbon production has real consequences for selecting the optimal ways of decreasing carbon emissions. A pressing necessity to control these carbon emissions is needed. The preliminary step is to precisely recognize the milestones and threat levels. Specific thresholds should be mapped that formulate the maximum levels of CO2 namely – the point of no return, risk point, and so on. This article focuses on the development of Multiple Attribute Group Decision-Making with Neutrosophic Environment for Carbon Emission Prediction (MAGDM-NECEP) method on Sustainable Urban Management. The MAGDM-NECEP architecture proficiently manages the multi-criteria nature of emission calculation, while neutrosophic logic accommodates ambiguity and uncertainty in input dataset. Furthermore, GSO enhances model parameters, improving prediction performance. The MAGDM synergy and neutrosophic logic offer strong decision-making abilities, whereas GSO fine-tuned the model parameter for superior outcomes. Empirical analysis establishes the efficiency of the presented technique in precisely predicting carbon emission, providing valuable insight for the environmentalist and policymaker in developing efficient mitigation strategy

Keywords: Carbon Emission Prediction; Neutrosophic Logic; GSO; Machine Learning; Deep Learning

1. Introduction

The foremost reason for weather change and varying earth temperature is CO2 emission. Gas presence in atmosphere fluctuates at one time or another. Few gases remain for some and many years [1]. Few gases are generally considered as more dangerous than the others. As per the study directed by Intergovernmental Panel on Climate Change, the ocean and land temperature was enlarged by an average of 0.85°C. Therefore, in the last 3 years, the emission of gases was high. It has reduced quantity of cold nights and days and improved quantity of hot nights and days [2]. Carbon dioxide (CO2) is more scrupulous for the effect of Green House. Generally, there are dissimilar features for CO2 emission like fermentation, burning of coal, oil, trees, wood products, solid waste, living organisms, and natural gas [3]. We can realize that the accessible online site for the residence of carbon calculators, carbon footprint, carbon offsetting, caring for the weather and CO2 reduction [4]. The development of the economy, CO2 emissions and energy utilization are extremely associated with each other. The authors point out that while the usage of resources like energy contains a bright side to development, it has harmful environmental effects [5]. Traditional evolution models such as the Solow growth method failed to reflect the environmental effects of growth. More current growth models study the interrelationship between environment, energy, and economic growth [6].

CO2 forecasts are generally vital in industries directly correlated to heavy energy production/ consumption [7]. The forecast of carbon emissions and energy consumption is vital to help a corporation's energy development and

Doi: https://doi.org/10.54216/IJNS.240127
Received: February 25, 2024 Revised: March 13, 2024 Accepted: April 02, 2024

carbon efficacy actions. For these reasons, time-sequence dataset is highly vital. Statistical and semi-hybrid techniques like ARIMA (Auto-Regressive Integrated Moving Average) are employed for this reason. However, forecasts are implemented by deep learning (DL) and machine learning (ML) models [8]. DL and ML models are effective way so, their overviews were utilized in nearly every business from healthcare, and production to logistics and much more. In addition, these models have created their approach to being used for weather change [9]. Different from statistical techniques, they deliver an edge over simple arithmetical models by employing many features and systems. ML and DL approaches form numerous mathematical and computerized techniques acquired from the data delivered and forecast prospect values [10]. ML and DL systems deliver very precise outcomes which delivered that they were modelled consequently.

This article focuses on the development of Multiple Attribute Group Decision-Making with Neutrosophic Environment for Carbon Emission Prediction (MAGDM-NECEP) method on Sustainable Urban Management. The MAGDM-NECEP architecture proficiently manages the multi-criteria nature of emission calculation, while neutrosophic logic accommodates ambiguity and uncertainty in input dataset. Furthermore, GSO enhances model parameters, improving prediction performance. The MAGDM synergy and neutrosophic logic offer strong decision-making abilities, whereas GSO fine-tuned the model parameter for superior outcomes. Empirical analysis establishes the efficiency of the presented technique in precisely predicting carbon emission, providing valuable insight for the environmentalist and policymaker in developing efficient mitigation strategy.

2. Related Works

In [11], a new carbon emission forecasting structure is developed for uniting linear and ML methods which reflects both exterior influences and time dynamics. The method at first presents 12 initial influencing features. A united forecast method by incorporating Support Vector Regression (SVR) and Autoregressive Integrated Moving Average (ARIMA) techniques has been recognized to capture non-linear and linear features, correspondingly. Kong et al. [12] utilize the identity of Kaya united with the logarithmic mean Divisia index (LMDI) decay model to analyse the factors disturbing carbon emission and employ the correlation coefficient to depart from 8 extremely linked features to build a prolonged STIRPAT method. This work presented the Adaboost model from Ml to improve the STIRPAT method. Lastly, scenario analysis is employed for predicting and analysing CO2 productions. Luo et al. [13] used the GM and the Mind Evolution Algorithm (MEA) techniques to enhance the BP neural networks method and estimate CO2 productions. The technique assessed carbon emission utilizing the lifecycle valuation model and IPCC carbon emission coefficient model. Moreover, the STIRPAT and Principal Component Analysis (PCA) techniques are employed to pick and decrease significant parameters, recognizing 3 principal components. Then, the MEA-BP approach has been used.

In [14], a model dependent upon the BiLSTM-CNN-GAN technique is projected. The BiLSTMCNN-GAN technique is a mixture of 3 DL models such as CNN, BiLSTM, and Generative Adversarial Networks (GAN). The Bi-LSTM module is utilized to procedure past data and remove time-sequence data, whereas the CNN module eliminates local structural and spatial feature data in urban carbon emissions and energy consumption data. Luo et al. [15] begin a Multi-universe Quantum Harmony Search-Algorithm Dynamic Fuzzy System Ensemble (MUQHS-DMFSE) composite method. This technique unites the MUQHS system with the DMFSE model by planning the working flow of the MUQHS model, generating the DMFSE composite forecast method, presenting a sliding factor matrix, and utilizing the MUQHS system to hunt for the optimum sliding factor. This study uses the Data Envelopment Analysis (DEA) model and creates Banker-Charnes-Cooper (BCC) and Charnes-Cooper-Rhodes (CCR) techniques. Ding et al. [16] reflect the effect of time-lag and interface effect of the manipulating factors on CO2 productions at the same time and form a novel grey multi-variate coupled model (CTGM) for CO2 productions forecast by presenting the grey multi-variate delay and Choquet fuzzy integral model. The whale optimizer algorithm (WOA) was intended to obtain the optimum parameter and precision of the method. The novel technique is planned for suitable data on carbon emission.

Doi: https://doi.org/10.54216/IJNS.240127
Received: February 25, 2024 Revised: March 13, 2024 Accepted: April 02, 2024

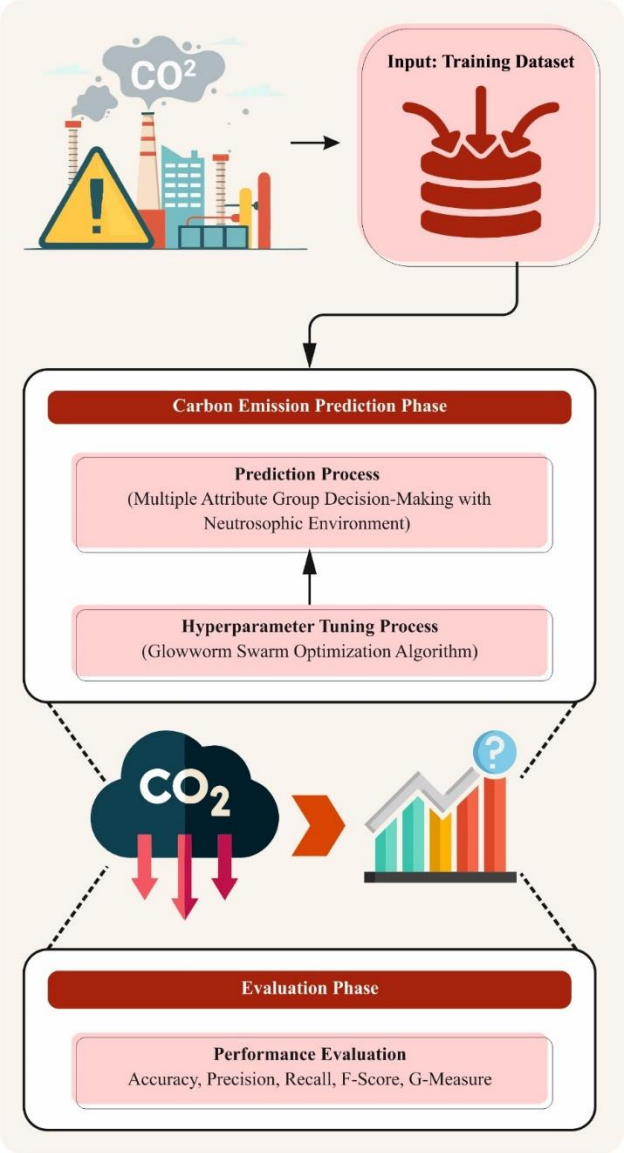

Figure 1: Overall flow of MAGDM-NECEP method

3. The Proposed Model

In this article, we focus on the desgin of MAGDM-NECEP method for sustainable urban management. The MAGDM-NECEP architecture proficiently manages the multi-criteria nature of emission calculation, while neutrosophic logic accommodates ambiguity and uncertainty in input dataset. Fig. 1 represents the entire flow of MAGDM-NECEP method.

A. Parameter Tuning

In an algorithm of GSO, the swarm is named a cluster of glowworms (GW) that are spread in the search space at random [17]. The particular GW directs a radiant amount such as luciferin. In addition, the GW is also capable of making their individual choices in decision area $GM_e^g\left(0 < GM_e^g \leq GM_u\right)$. The tactic behind the contact between GW is given in the following: the light power of GW is equivalent to related luciferin directly, and contact with other GW, that is obtainable in flexible neighborhoods. Besides, the luciferin strength has been significantly related to the current location. The position of the optimal GW is recognized if and only if, the strength of luciferin is higher. Presume a g GW, and w specifies its adjacent GW if and only if w is in its range of neighborhood. Fig. 2 represents the flowchart of GSO.

Generally, the neighborhood is definite as the local decision area beside GM_e^g, which arrays the radial sensor range $GM_u\left(0 < GM_e^g \leq GM_u\right)$. The GW range is in an exact format: the neighborhood GW with maximal value of

Doi: https://doi.org/10.54216/IJNS.240127
Received: February 25, 2024 Revised: March 13, 2024 Accepted: April 02, 2024

luciferin than existing GW is preferred and ahead near it. Normally, the algorithm of GSO contains 4 phases such as initialize, luciferin-update, movement and update of neighborhood range.

Phase 1: Initialize

Here, the GW is spread throughout the search range at random. Then, the GW have same luciferin strength with parallel decision area GM_0.

Phase 2: Luciferin-Update

Generally, the luciferin strength of GW is very connected to the fitness position's. When the strength value is bigger, it gets the optimal location. Or else, it is measured as poor. The GW's location acquires diverse once the iteration rises and the luciferin value is upgraded mechanically. The g GW location at r time is $X_g(t)$ and the linked value of objective function at g^{th} GW position at t is $(X_g(t))$. Additionally, put $J\left(X_g(t)\right)$ to $LU_g(t)$, which represents the luciferin level that is connected to g glow- worm at t and it is definite in Eq. (1), in which 0 states the luciferin deterioration constant $(0 < \mathrm{v} < 1)$, η denotes the luciferin enhancement constant.

$$LU_g(t) = (1 - \mathrm{v})LU_g(t-1) + \eta\left(J\left(X_g(t)\right)\right) \quad (1)$$

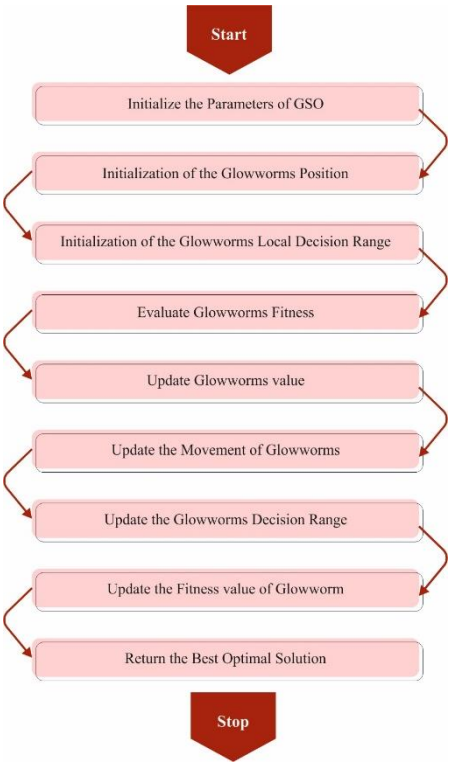

Figure 2: Flowchart of GSO

Phase 3: Movement

In this stage, all the GW pick their neighbor and track it with a typical prospect. The neighbor GW of g wants to fulfil dual needs: At first, GW at the decision area of g GW; additional is that the luciferin value must be larger than the g GW value. Besides, g GW travels near w neighbor that starts from $N_g(t)$ with a committed probability $PT_{gj}(t)$, and it is conveyed as assumed in Eq. (2).

$$PT_{gj}(t) = \frac{LU_w(t) - LU_g(t)}{\sum_{I \epsilon W_g(ti)} L\,U_l(t) - LU_g(t)} \quad (2)$$

Once the movement of g GW occurs, the location acquires upgraded and the valuation of location upgrade has been specified in Eq. (3), whereas size specifies the size of step.

Doi: https://doi.org/10.54216/IJNS.240127
Received: February 25, 2024 Revised: March 13, 2024 Accepted: April 02, 2024

$$X_g(t+1) = X_i(t) + size * \left(\frac{X_w(t) - X_g(t)}{\left\| X_w(t) - X_g(t) \right\|} \right) \quad (3)$$

Phase 4: Update of neighborhood area.

After upgrading the GW position, it tracks the upgrade of range of neighborhood. If the neighborhood area refuges up tiny GW compactness, then it gets higher or else reduced. The upgrade formulation is set in Eq. (4), whereas λ specifies the constant parameter. Where, nu_t has been marked as the parameter to handle neighbors amount.

$$GM_e^g(t+1) = \min\left\{ GM_u, \max\left\{0, GM_e^g(t) + \lambda \left| N_g(t) \right| \right\} \right\} \quad (4)$$

The GSO model is used to derive an FF for obtaining superior classifier results. It describes a positive integer to characterize the high efficiency of solution candidate. Now, the decline of classifier error is assumed as the FF.

$$fitness(x_i) = ClassifierErrorRate(x_i)$$
$$= \frac{No.of\ misclassified\ samples}{Total\ No.of\ samples} * 100 \quad (5)$$

B. Design of MAGDM Method

The MAGDM synergy and neutrosophic logic offer strong decision-making abilities, whereas GSO fine-tuned the model parameter for superior outcomes.

A Vague set V on the universe of dissertation X formulated by $A = \{< x, t_A(x), 1 - f_A(x) > | x \in X\}$. is considered as a $t_v$and f_v truth- and false-membership functions [18].

$t_v: U \to [O, 1]$, $f_v: U \to [O, 1]$, and $t_v + f_v \leq 1$

Assume A and B as vague sets for$A = \{< x, t_A(x), 1 - f_A(x) > | x \in X\}$ and $B = \{< x, t_B(x), 1 - f_B(x) > | x \in X\}$. Thus

i. A $\subseteq$ if and only if $t_A(x) \leq t(x)$ and $1 - f_A(x) \leq 1 - f_B(x)$.

ii. $A = B$ if and only if $A \subseteq B$ and $B \subseteq A$.

iii. $A^c = \{< x, 1 - f_A(x), t_A(x) > | x \in X\}$.

iv. $AB = \{< x,\ \max\left(t_A(x), t_B(x)\right),\ \max\left(1 - f_A(x), 1 - f_B(x)\right) > \left| x \in X\right\}$.

v. $A \cap B = \{< x, \min\left(t_A(x), t_B(x)\right), \min\left(1 - f_A(x), 1 - f_B(x)\right) > \left| x \in X\right\}$.

A neutrosophic set A on the universe of dissertation X is given below

$A = \{< x, T_A(x), I_A(x), F_A(x) >, x \in X\}$where $T, I, F: X \to]^-0, 1^+[and^- 0 \leq T_A(x) + I_A(x) + F_A(x) \leq 3^+$.

A neutrosophic vague set ANV (NVS) on the universe of dissertation X represented as $ANV = \{< x; TNV(X), INV(X), FNV(X) >; x \in X\}$ whose truth, indeterminacy and false-membership functions are written below:

$TNV\ (x) = [T^-, T^+], INV(x) = [I^-, I^+], FNV = [F^-, F^+]$ where

1) $T^+ = 1 - F^-$

2) $F^+ = 1 - T^-$ and

3) $0^- \leq T^- + I^- + F^- \leqq 2^+$.

Assume X as a universe of discourse. The bipolar neutrosophic set ANS in X is described by the object for $ANS = \{< x; T^+(x), I^+(x), F^+(x), T^-(x), I^-(x), F^-(x) >; x \in X\}$

Where $T^+, F^+, I^+: X \to [1,0]$ and $T^-, F^-, I^-: X \to [-1,0]$. Let $ANV = \{< x; TNV(X), INV(X), FNV(X) >; x \in X\}$and $BNV = \{< x; TNV(X), INV(X), FNV(X) >; x \in X\}$ two neutrosophic vague set in X. Next, the two Jaccard index measures of ANV and BNV are introduced according to the distance and weighted Jaccard index measure of two vectors, correspondingly

Doi: https://doi.org/10.54216/IJNS.240127
Received: February 25, 2024 Revised: March 13, 2024 Accepted: April 02, 2024

$$J_{NV}(A_{NV}, B_{NV}) =$$

$$\sum_{i=1}^{n}\left(\frac{\begin{matrix}[T^{+}_{ANV}(x_i).T^{+}_{BNV}(x_i)]+[T^{-}_{ANV}(x_i).T^{-}_{BNV}(x_i)]+[I^{+}_{ANV}(x_i).I^{+}_{BNV}(x_i)]+[I^{-}_{ANV}(x_i).I^{-}_{BNV}(x_i)]+[F^{+}_{ANV}(x_i)F^{+}_{BNV}(x_i)]\\ +[F^{-}_{ANV}(x_i).F^{-}_{BNV}(x_i)]\end{matrix}}{\begin{matrix}([T^{+}_{ANV}(x_i)]^2+[T^{+}_{BNV}(x_i)]^2+[T^{-}_{ANV}(x_i)]^2+[T^{-}_{BNV}(x_i)]^2+[I^{+}_{ANV}(x_i)]^2+[I^{+}_{BNV}(x_i)]^2+[I^{-}_{ANV}(x_i)]^2+[I^{-}_{BNV}(x_i)]^2)\\ +[F^{+}_{ANV}(x)]^2+[F^{+}_{BNV}(x_i)]^2+[F^{-}_{ANV}(x_i)]^2+[F^{-}_{BNV}(x_i)]^2),\\ -([T^{+}_{ANV}(x_i).T^{+}_{BNV}(x_i)]+[T^{+}_{ANV}(x_i).T^{+}_{BNV}(x_i)]+[I^{+}_{ANV}(x_i).I^{+}_{BNV}(x_i)]+[I^{-}_{ANV}(x_i).I^{-}_{BNV}(x_i)])\\ +[F_{ANV}(x_i)F_{BNV}(x_i)]+[F^{-}_{ANV}(x_i)F^{-}_{BNV}(x_i)])\end{matrix}}\right) \quad (6)$$

Weighted Jaccard index measure according to two vectors

$$WJ_{NV}(A_{NV}, B_{NV}) =$$

$$\sum_{i=1}^{n}(w_i)\left(\frac{\begin{matrix}[T^{+}_{ANV}(x_i).T^{+}_{BNV}(x_i)]+[T^{-}_{ANV}(x_i).T^{-}_{BNV}(x_i)]+[I^{+}_{ANV}(x_i).I^{+}_{BNV}(x_i)]+[I^{-}_{ANV}(x_i).I^{-}_{BNV}(x_i)]\\ +[F^{+}_{ANV}(x_i).F^{+}_{BNV}(x_i)]+[F^{-}_{ANV}(x_i).F^{-}_{BNV}(x_i)]\end{matrix}}{\begin{matrix}([T^{+}_{ANV}(x_i)]^2+[T^{+}_{BNV}(x_i)]^2+[\tau^{-}_{ANV}(x_i)]^2+[\tau^{-}_{BNV}(x_i)]^2+[I^{+}_{ANV}(x_i)]^2.+[I^{+}_{BNV}(x_i)]^2+[I_{\bar{A}NV}(x_i)]^2+[I^{-}_{BNV}(x_i)]^2)\\ +[F^{+}_{ANV}(x_i)]^2+[F^{+}_{BNV}(x_i)]^2[F_{\bar{A}NV}(x_i)]^2+[F^{-}_{BNV}(x_i)]^2,\\ -([T^{+}_{ANV}(x_i).T^{+}_{BNV}(x_i)]+[T^{-}_{ANV}(x_i).T^{-}_{BNV}(x_i)]+[I^{+}_{ANV}(x_i)]+[I^{-}_{ANV}(x_i).I^{-}_{BNV}(x_i)])\\ +[F^{+}_{ANV}(x_i).F^{+}_{BNV}(x_i)]+\left[F^{-}_{ANV}\left((x_i)F^{-}_{BNV}(x_i)\right]\right)\end{matrix}}\right)$$

The 2 Jaccard index measures $J(A_{NV}, B_{NV})$ for the NVs satisfy $(p1)$-$(p3)$:

(p1)$0 \le J_{NV}(A_{NV}, B_{NV}) \le 1$;

(p2)$J_{NV}(A_{NV}, B_{NV}) = J_{NV}(B_{NV}, A_{NV})$;

(p3) If $A_{NV} = B_{NV}$, then $J_{NV}(A_{NV}, B_{NV}) = 1$.

First, we prove $(p1) - (p3)$ of $J(A_{NV}, B_{NV})$

$(p1)$ clearly $J_{NV}(A_{NV}, B_{NV}) \ge 0$

we must prove $J_{NV}(A_{NV}, B_{NV}) \le 1$ by the inequality

$2ab \le a^2 + b^2$.

$+Tab[-\|.-()]+[Tab0\ \|.0\ \|]$

$$\Sigma_{i=1}^{n}\left(\begin{matrix}[T^{+}_{ANV}(x_i).T^{+}_{BNV}(x_i)]+[T^{-}_{ANV}(x_i).T^{-}_{BNV}(x_i)]+[I^{+}_{ANV}(x_i).I^{+}_{BNV}(x_i)]+[I^{-}_{ANV}(x_i).I^{-}_{BNV}(x_i)]\\ +[F^{+}_{ANV}(x_i).F^{+}_{BNV}(x_i)]+[F^{-}_{ANV}(x_i).F^{-}_{BNV}(x_i)]\end{matrix}\right) \le$$

$$\Sigma_{i=1}^{n}\left(\begin{matrix}\left(\begin{matrix}[T^{+}_{ANV}(x_i)]^2+[T^{+}_{BNV}(x_i)]^2+[T^{-}_{ANV}(x_i)]^2+[[T^{+}_{BNV}(x_i)]^2+[I^{+}_{ANV}(x_i)]^2.[I^{+}_{BNV}(x_i)]^2+\\ [I^{-}_{ANV}(x_i)]^2+[I^{-}_{BNV}(x_i)]^2+[F^{+}_{ANV}(x_i)]^2+[F^{+}_{BNV}(x_i)]^2+[F^{-}_{ANV}(x_i)]^2+\{F^{-}_{BNV}(x_i)]^2\end{matrix}\right)\\ -\left(\begin{matrix}[T^{+}_{ANV}(x_i).T^{+}_{BNV}(x_i)]+[T^{-}_{ANV}(x_i).T^{-}_{BNV}(x_i)]+[I^{+}_{ANV}(x_i).I^{+}_{BNV}(x_i)]+[I^{-}_{ANV}(x_i).I^{-}_{BNV}(x_i)]\\ +[F^{+}_{ANV}(x_i).F^{+}_{BNV}(x_i)]+[F^{-}_{ANV}(x_i).F^{-}_{BNV}(x_i)]\end{matrix}\right)\end{matrix}\right)$$

$$\sum_{i=1}^{n}\left(\frac{\begin{matrix}[T^{+}_{ANV}(x_i).T^{+}_{BNV}(x_i)]+[T^{-}_{ANV}(x_i)..T^{-}_{BNV}(x_i)]+[I^{+}_{ANV}(x_i).I^{+}_{BNV}(x_i)]+\\ [I^{-}_{ANV}(x_i).I^{-}_{BNV}(x_i)]+[F^{+}_{ANV}(x_i)F^{+}_{BNV}(x_i)]+[F^{-}_{ANV}(x_i).F^{-}_{BNV}(x_i)]\end{matrix}}{\begin{matrix}\left(\begin{matrix}[T^{+}_{ANV}(x_i)]^2+[T^{+}_{BNV}(x_i)]^2+[T^{-}_{ANV}(x_i)]^2+[[T^{+}_{BNV}(x_i)]^2+[I^{+}_{ANV}(x_i)]^2.[I^{+}_{BNV}(x_i)]^2+\\ [I^{-}_{ANV}(x_i)]^2+[I^{-}_{BNV}(x_i)]^2+[F^{+}_{ANV}(x_i)]^2+[F^{+}_{BNV}(x_i)]^2+[F^{-}_{ANV}(x_i)]^2+[F^{-}_{BNV}(x_i)]^2\end{matrix}\right)\\ -\left(\begin{matrix}[T^{+}_{ANV}(x_i).T^{+}_{BNV}(x_i)]+[T^{-}_{ANV}(x_i).T^{-}_{BNV}(x_i)]+[I^{+}_{ANV}(x_i).I^{+}_{BNV}(x_i)]+[I^{-}_{ANV}(x_i).I^{-}_{BNV}(x_i)]\\ +[F^{+}_{ANV}(x_i).F^{+}_{BNV}(x_i)]+[F^{-}_{ANV}(x_i).F^{-}_{BNV}(x_i)]\end{matrix}\right)\end{matrix}}\right) \le 1$$

$$\therefore J_{NV}(A_{NV}, BNV) \le 1$$

Doi: https://doi.org/10.54216/IJNS.240127
Received: February 25, 2024 Revised: March 13, 2024 Accepted: April 02, 2024

Thus, $0 \leq J_{NV}(A_{NV}, BNV) \leq 1$ holds.

$(p2)$ It is clear that

$J_{NV}(A_{NV}, BNV) = J_{NV}(B_{NV}, ANV)$,

$\therefore$ It is true.

(p3) $if\, A_{NV} = B_{NV}$,

$(T_{AN}^{+}v(xi), TANV(X);\ I^{+}ANV(Xi), I_{ANV}^{-}(Xi); F_{AN}^{+}v(Xi), F_{ANV}^{-}(Xi)) =$
$(T_{BN}^{+}v(xi), TBNV(X);\ I_{BN}^{+}v(xi), IBNV(X)\ ; F_{BN}^{+}v(xi), F_{BN}^{-}v(x))$

where $i = 1,2,3 \ldots \ldots \ldots, n$.

Now, AV and BNV are two vectors so,

$\|A_{NV}\| = \|B_{NV}\|$ where

$$\|A_{NV}\| = \sqrt{[T_{ANV}^{+}(x_i)]^2 + [T_{ANV}^{-}(x_i)]^2 + [l_{ANV}^{+}(x_i)]^2 + [l_{ANV}^{-}(x_i)]^2 + [F_{ANV}^{+}(x_i)]^2 + [F_{ANV}^{-}(x_i)]^2}$$

$$\|B_{NV}\| = \sqrt{[T_{BNV}^{+}(x_i)]^2 + [T_{BNV}^{-}(x_i)]^2 + [l_{BNV}^{+}(x_i)]^2 + [l_{BNV}^{-}(x_i)]^2 + [F_{BNV}^{+}(x_i)]^2 + [F_{BNV}^{-}(x_i)]^2}$$

And there are $\frac{A_{NV}.B_{NV}}{||A_{NV}||.||B_{NV}||}$

$$\frac{\begin{matrix}-[T_{ANV}^{+}(x_i).T_{BNV}^{+}(x_i)]+[T_{ANV}^{-}(x_i)T_{BNV}^{-}(x_i)]+[I_{ANV}^{+}(x_i)(_i x_{X_i})]+[I_{ANV}^{-}(x_i)I_{BNV}^{-}(x_i)] \\ +[F_{ANV}^{+}(x_i).F_{BNV}^{+}(x_i).]+[F_{ANV}^{-}(x_i).F_{BNV}^{-}(x_i)]\end{matrix}}{\begin{matrix}\sqrt{[T_{ANV}^{+}(x_i)]^2+[T_{ANV}^{-}(x_i)]^2+[l_{ANV}^{+}(x_i)]^2+[l_{ANV}^{-}(x_i)]^2+[F_{ANV}^{+}(x_i)]^2+[F_{ANV}^{-}(x_i)]^2.} \\ \sqrt{[T_{BNV}^{+}(x_i)]^2+[T_{BNV}^{-}(x_i)]^2+[l_{BNV}^{+}(x_i)]^2+[l_{BNV}^{-}(x_i)]^2+[F_{BNV}^{+}(x_i)]^2+[F_{BNV}^{-}(x_i)]^2}\end{matrix}} = 1.$$

Therefore,

$$J_{NV}(A_{NV}, B_{NV}) = 1.$$

Hence, we proved. Assume the weighted Jaccard index measure between AV and B_{NV}, correspondingly, as follows:

$$WJ_{NV}(A_{NV}, B_{NV})$$

$$= \sum_{i=1}^{n}(w_i)\left(\begin{matrix}\begin{matrix}[T_{ANV}^{+}(x_i).T_{BNV}^{+}(x_i)] + [T_{ANV}^{-}(x_i)..T_{BNV}^{-}(x_i)] + [I_{ANV}^{+}(x_i).I_{BNV}^{+}(x_i)] + \\ [I_{ANV}^{-}(x_i).I_{BNV}^{-}(x_i)] + [F_{ANV}^{+}(x_i)F_{BNV}^{+}(x_i)] + [F_{ANV}^{-}(x_i).F_{BNV}^{-}(x_i)]\end{matrix} \\ \hline \begin{matrix}\left(\begin{matrix}[T_{ANV}^{+}(x_i)]^2 + [T_{BNV}^{+}(x_i)]^2 + [T_{ANV}^{-}(x_i)]^2 + [[T_{BNV}^{+}(x_i)]^2 + [I_{ANV}^{+}(x_i)]^2.[I_{BNV}^{+}(x_i)]^2 + \\ [I_{ANV}^{-}(x_i)]^2 + [I_{BNV}^{-}(x_i)]^2 + [F_{ANV}^{+}(x_i)]^2 + [F_{BNV}^{+}(x_i)]^2 + [F_{ANV}^{-}(x_i)]^2 + [F_{BNV}^{-}(x_i)]^2\end{matrix}\right) \\ -\left(\begin{matrix}[T_{ANV}^{+}(x_i).T_{BNV}^{+}(x_i)] + [T_{ANV}^{-}(x_i).T_{BNV}^{-}(x_i)] + [I_{ANV}^{+}(x_i).I_{BNV}^{+}(x_i)] + [I_{ANV}^{-}(x_i).I_{BNV}^{-}(x_i)] \\ +[F_{ANV}^{+}(x_i).F_{BNV}^{+}(x_i)] + [F_{ANV}^{-}(x_i).F_{BNV}^{-}(x_i)]\end{matrix}\right)\end{matrix}\end{matrix}\right)$$

Where $Wi \in [0,1]$, and $\sum_{i=1}^{n} w_i = 1$ for $i = 1,2, \ldots, n$.

The weighted Jaccard index measures $WJ(A_{NV}, BNV)$ statisfy the $(p1)$-$(p3)$:

(p1)$0 \leq WJ_{NV}(A_{NV}, BNV) \leq 1$;

(p2)$WJ_{NV}(A_{NV}, BNV) = WJ_{NV}(B_{NV}, ANV)$;

(p3) If $A_{NV} = B_{NV}$, then $WJ_{NV}(A_{NV}, B_{NV}) = 1$.

We prove $(p1) - (p3)$ for $WJ_{NV}(A_{NV}, B_{NV})$.

Doi: https://doi.org/10.54216/IJNS.240127
Received: February 25, 2024 Revised: March 13, 2024 Accepted: April 02, 2024

For the MAGDM problems, consider $G = \{g_1, g_2, \cdots g_m\}$ and $A = \{A_1, A2\ \cdots A_n\}$ a set of m and n attributes. The weight vector of the attributes $Aj\ (j = 1,2,,n)$ is $\omega A = (\omega A1, \omega A2,, \omega An)^T$, satisfy$\omega Aj \in [0,1]$, and $\sum_{j=1}^{n} \omega_{Aj} = 1$ for $j = 1,2,\dots,n$. Consider that $EX = \{EX, EX, \dots, EX\}$ is a grou=1specialist and the weight vector is $\omega_E = (\omega_{E1}, \omega_{E2},, \omega_{Ey})^T$, satisfy $\omega_E k[0, 1]$, and $\sum_{k=1}^{y} \omega_{Ek} = 1$. The specialist can allocate the degree of truth-, falsity, and indeterminacy functions to $A_j(j = 1,2,\dots,n)$ on the selections $g_i(i = 1,2,\dots,m)$ based on the neutrosophic environment correspondingly.

$D^k = \left(d_{i,j}^k\right)m \times n = [D_1^k, D_2^k,., D_m^k]^T$, is an NVs for TNV, INV, $F_{NV} \in [O, 1]$

Next, the Jaccard index measure of neutrosophic vague set is to resolve the MAGDM problem.

Step 1: We establish the Ns, BNs, NVs matrix $G_{H^*} = (g_{i,j}^*)_{4x3} G_i^*\ (i = 1,2,3,4)$:

$$G_{H^k} = \left(g_{i,j}^k\right)m \times n = [G_1^k, G_2^k,., G_m^k]^T$$

Step 2: Evaluate the weighted Jaccard index measures values using H.

Step 3: Evaluate the weighted Jaccard index measure value to assess the alternatives $G_i\ (i = 1,2,,m)$.

$$J_H(D^k, G_i) = \sum_{k=1}^{y} \omega_{Ek} J_H\left(D_i^k, G_i\right) \tag{8}$$

$$WJ_H(D^k, G_i) = \sum_{k=1}^{y} \omega_{Ek} J_H\left(D_i^k, G_i\right) \tag{9}$$

Where $\omega_{Ek} \in [0,1]$ and $\sum_{k=1}^{y} \omega_{Ek} = 1$.

Step 4: Rank each alternative based on the $WJ_H(D^k, G_i)$ or $J_H(D^k, G_i)$ and choose the best option.

Step 5: End.

4. Result Analysis

This section inspects the performance of the MAGDM-NECE technique on carbon emission dataset. It contains 600 samples with 6 classes as depicted in Table 1.

Table 1: Details of dataset

Classes	No. of Instances
Good	100
Satisfactory	100
Moderate	100
Poor	100
Very Poor	100
Severe	100
Total Instances	600

The performance of the MAGDM-NECE model on test data is validated in Fig. 3. The confusion matrices presented by the MAGDM-NECE system on 70%TRAS and 30%TESS are described in Figs. 3a-3b. The outcome specified that the MAGDM-NECE model has precisely recognized and categorized all 6 classes. Similarly, the PR examination of the MAGDM-NECE model is established in Fig. 3c. The figure shows that the MAGDM-NECE model has gained high PR value on each class label. Finally, the ROC investigation of the MAGDM-NECE method is exemplified in Fig. 3d. The figure shows that the MAGDM-NECE technique has led to positive outcomes with highest ROC performances on various classes.

Doi: https://doi.org/10.54216/IJNS.240127
Received: February 25, 2024 Revised: March 13, 2024 Accepted: April 02, 2024

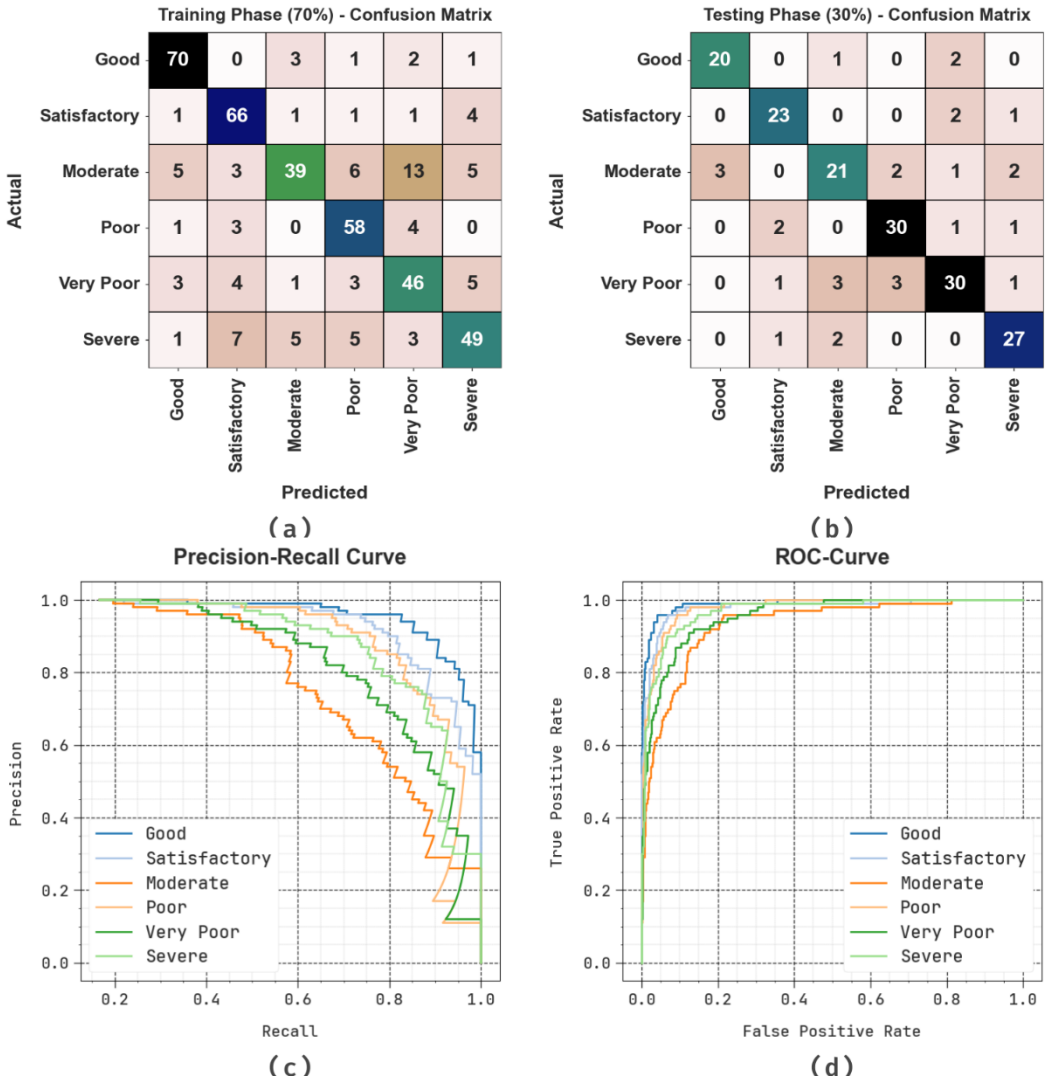

Figure 3: Classifier results of (a-b) 70% and 30% of confusion matrices and (c-d) PR and ROC analysis

The performance of the MAGDM-NECE model are shown in Table 2 and Fig. 4. The results suggest that the MAGDM-NECE technique properly identified various classes. With 70%TRAS, the MAGDM-NECE method attains average $accu_y$ of 92.70%, $prec_n$ of 77.86%, 77.85%, 77.32%, and 77.58%, correspondingly. Additionally, with 30%TESS, the MAGDM-NECE method attains average $accu_y$ of 94.63%, $prec_n$ of 83.89%, 84.17%, 83.98%, and 84.01%, correspondingly.

Table 2 Recognition outcome of MAGDM-NECE technique under 70%TRAS and 30%TESS

Classes	$Accu_y$	$Prec_n$	$Reca_l$	F_{Score}	$G_{Measure}$
TRAS (70%)					
Good	95.71	86.42	90.91	88.61	88.64
Satisfactory	94.05	79.52	89.19	84.08	84.21
Moderate	90.00	79.59	54.93	65.00	66.12
Poor	94.29	78.38	87.88	82.86	82.99
Very Poor	90.71	66.67	74.19	70.23	70.33
Severe	91.43	76.56	70.00	73.13	73.21

Doi: https://doi.org/10.54216/IJNS.240127
Received: February 25, 2024 Revised: March 13, 2024 Accepted: April 02, 2024

Average	92.70	77.86	77.85	77.32	77.58
TESS (30%)					
Good	96.67	86.96	86.96	86.96	86.96
Satisfactory	96.11	85.19	88.46	86.79	86.81
Moderate	92.22	77.78	72.41	75.00	75.05
Poor	95.00	85.71	88.24	86.96	86.97
Very Poor	92.22	83.33	78.95	81.08	81.11
Severe	95.56	84.38	90.00	87.10	87.14
Average	94.63	83.89	84.17	83.98	84.01

The classifier outcomes of the MAGDM-NECE method are graphically shown in Fig. 5 in the form of training accuracy (TRAA) and validation accuracy (VALA). The outcome displays valuable analysis of the behavior of the MAGDM-NECE model over different epochs, indicating its generalization capabilities and learning process. Notably, the figure indicates a constant development in the TRAA and VALA with increasing epoch count. It ensures the adaptable nature of the MAGDM-NECE model in the pattern detection model on both datasets. The increasing tendency in VALA describes the capability of the MAGDM-NECE model to adapt to the TRA dataset and excel in providing correct classifier of hidden dataset, showing the strong generalisability.

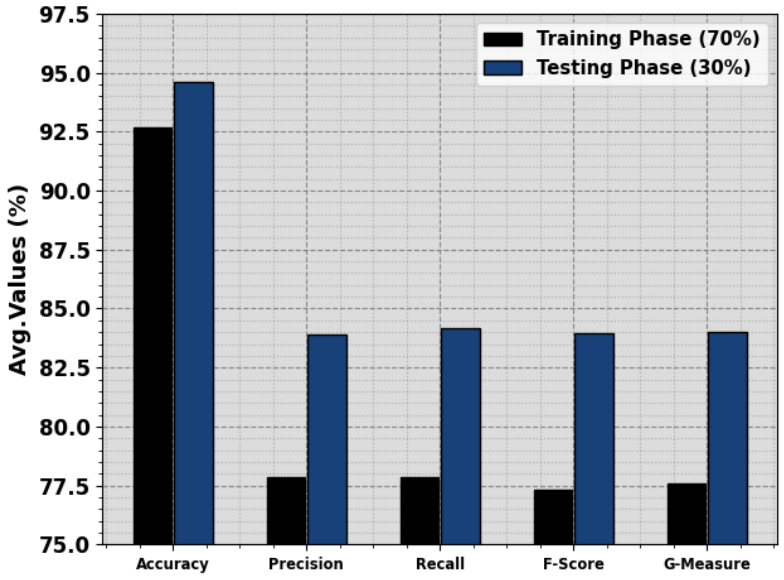

Figure 4: Average of MAGDM-NECE technique under 70%TRAS and 30%TESS

Doi: https://doi.org/10.54216/IJNS.240127
Received: February 25, 2024 Revised: March 13, 2024 Accepted: April 02, 2024

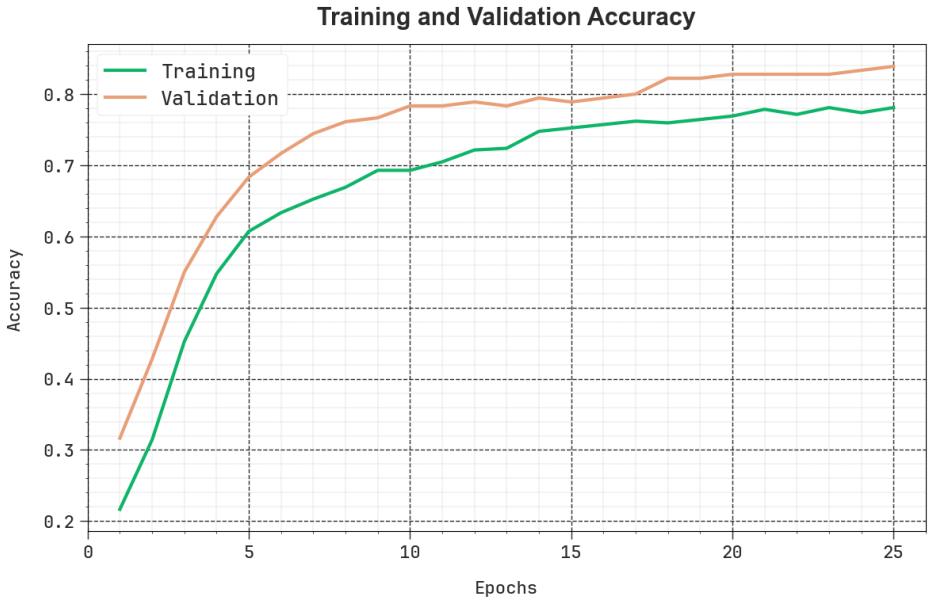

Figure 5: $Accu_y$ curve of the MAGDM-NECE technique

Fig. 6 exhibits a comprehensive review of the training loss (TRLA) and validation loss (VALL) results of the MAGDM-NECE technique over dissimilar epoch counts. The progressive decline in TRLA highlights the MAGDM-NECE method enhancing the weights and reducing the classification error on both datasets. The figure demonstrates a clear insight of the MAGDM-NECE model's relationship with the TRA dataset, which highlights its ability to capture patterns within both datasets. Notably, the MAGDM-NECE method recurrently increases its parameters in diminishing the variances amongst the prediction and real TRA classes.

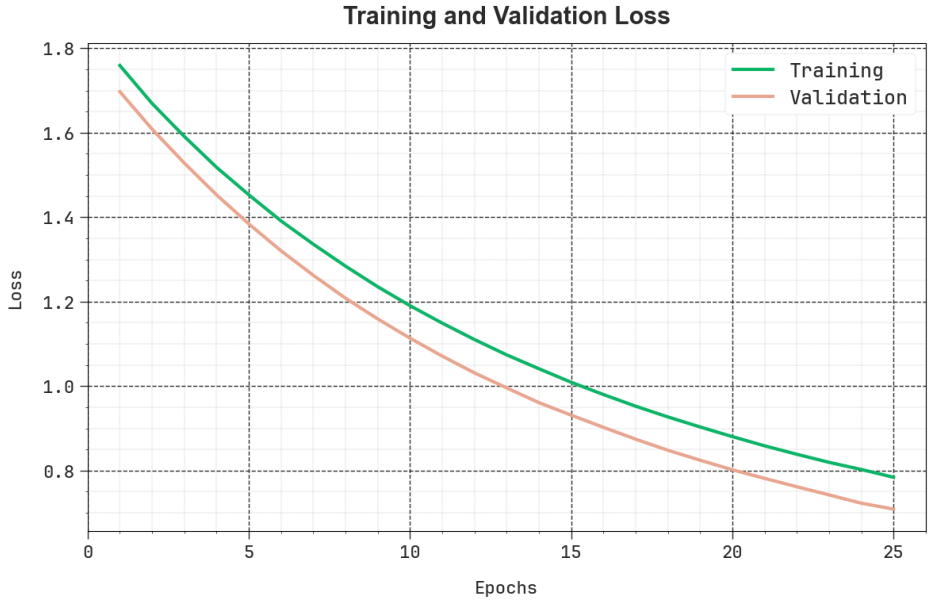

Figure 6: Loss curve of the MAGDM-NECE technique

The performance of the MAGDM-NECE technique is compared with other models in Table 3 and Fig. 7. Based on $accu_y$, the MAGDM-NECE technique offers increased $accu_y$ of 94.63% while the RF, KNN, VGG16, Inception v3, LSTM, and CNN models attain decreased $accu_y$ of 89.64%, 91.20%, 90.65%, 93.13%, 91.26%, and 92.71%, correspondingly. Also, based on $prec_n$, the MAGDM-NECE method provides better $prec_n$ of 83.89% while the RF, KNN, VGG16, Inception v3, LSTM, and CNN technique obtain reduced $prec_n$ of 79.73%, 81.13%, 78.55%, 78.65%, 80.53%, and 77.21%, correspondingly. Moreover, based on $reca_l$, the MAGDM-NECE method provides improved $reca_l$ of 84.17% while the RF, KNN, VGG16, Inception v3, LSTM, and CNN techniques obtain reduced $reca_l$ of 77.67%, 81.18%, 79.33%, 82.91%, 82.64%, and 82.20%, correspondingly. Finally, based on F_{score}, the MAGDM-NECE model provides superior F_{score} of 83.98% while the RF, KNN, VGG16,

Doi: https://doi.org/10.54216/IJNS.240127
Received: February 25, 2024 Revised: March 13, 2024 Accepted: April 02, 2024

Inceptionv3, LSTM, and CNN techniques obtain reduced F_{score} of 79.12%, 82.27%, 78.46%, 82.27%, 82.34%, and 77.60%, correspondingly. Accordingly, the MAGDM-NECE model can be exploited for enhanced results.

Table 3. Comparative analysis of MAGDM-NECE technique with recent algorithms

Method	$Accu_y$	$Prec_n$	$Reca_l$	F_{Score}
Random Forest	89.64	79.73	77.67	79.12
KNN Algorithm	91.20	81.13	81.18	82.27
VGG16 Model	90.65	78.55	79.33	78.46
InceptionV3	93.13	78.65	82.91	82.27
LSTM Model	91.26	80.53	82.64	82.34
CNN Model	92.71	77.21	82.20	77.60
MAGDM-NECE	94.63	83.89	84.17	83.98

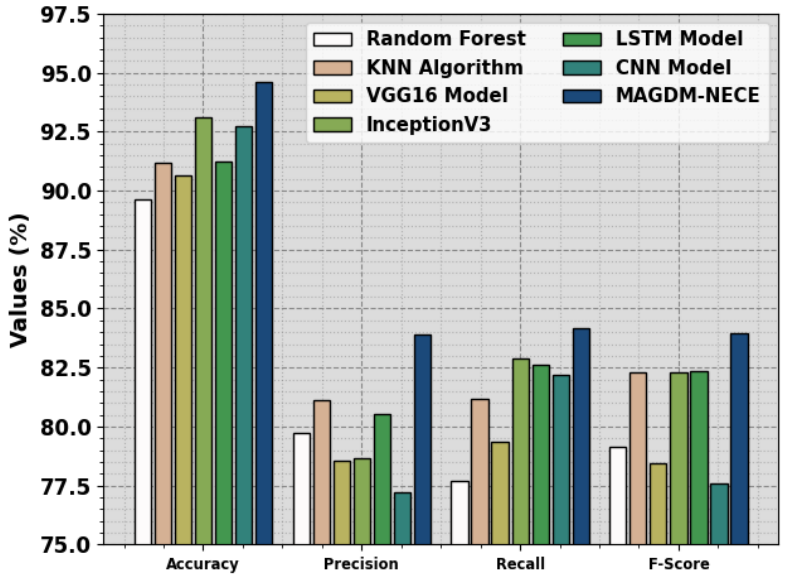

Figure 7: Comparative analysis of MAGDM-NECE model with existing algorithms

5. Conclusion

In this article, we focus on the development of MAGDM-NECEP method for sustainable urban management. The MAGDM-NECEP architecture proficiently manages the multi-criteria nature of emission calculation, while neutrosophic logic accommodates ambiguity and uncertainty in input dataset. Furthermore, GSO enhances model parameters, improving prediction performance. The MAGDM synergy and neutrosophic logic offer strong decision-making abilities, whereas GSO fine-tuned the model parameter for superior outcomes. Empirical analysis establishes the efficiency of the presented technique in precisely predicting carbon emission, providing valuable insight for the environmentalist and policymaker in developing efficient mitigation strategy.

Funding: "The author extends his appreciation to Prince Sattam bin Abdulaziz University for funding this research work through the project number (PSAU/ 2024/01/27506)"

Conflicts of Interest: "The authors declare no conflict of interest."

References

[1] Manvitha, M.S.; Vani Pujitha, M.; Prasad, N.H.; Yashitha Anju, B. A Predictive Analysis on CO2 Emissions in Automobiles using Machine Learning Techniques. In Proceedings of the 2023 International Conference

Doi: https://doi.org/10.54216/IJNS.240127
Received: February 25, 2024 Revised: March 13, 2024 Accepted: April 02, 2024

on Intelligent Data Communication Technologies and Internet of Things (IDCIoT), Bengaluru, India, 5–7 January 2023; pp. 394–401.
[2] Li, G.; Yang, Z.; Yang, H. A new hybrid short-term carbon emissions prediction model for aviation industry in China. Alex. Eng. J. 2023, 68, 93–110.
[3] Khajavi, H.; Rastgoo, A. Predicting the carbon dioxide emission caused by road transport using a Random Forest (RF) model combined by Meta-Heuristic Algorithms. Sustain. Cities Soc. 2023, 93, 104503.
[4] Amarpuri, L.; Yadav, N.; Kumar, G.; Agrawal, S. Prediction of CO2 emissions using deep learning hybrid approach: A Case Study in Indian Context. In Proceedings of the 2019 Twelfth International Conference on Contemporary Computing (IC3), Noida, India, 8–10 August 2019; pp. 1–6.
[5] Meng, Y.; Noman, H. Predicting CO2 Emission Footprint Using AI through Machine Learning. Atmosphere 2022, 13, 1871.
[6] Ma, N.; Shum, W.Y.; Han, T.; Lai, F. Can Machine Learning be Applied to Carbon Emissions Analysis: An Application to the CO2 Emissions Analysis Using Gaussian Process Regression. Front. Energy Res. 2021, 9, 756311.
[7] Kumari, S.; Singh, S.K. Machine learning-based time series models for effective CO2 emission prediction in India. Environ. Sci. Pollut. Res. 2022.
[8] Cansiz, O.F.; Unsalan, K.; Unes, F. Prediction of CO2 emission in transportation sector by computational intelligence techniques. Int. J. Glob. Warm. 2022, 27, 271.
[9] Khan, M.Z.; Khan, M.F. Application of ANFIS, ANN and fuzzy time series models to CO2 emission from the energy sector and global temperature increase. Int. J. Clim. Chang. Strateg. Manag. 2019, 11, 622–642.
[10] Chai, H.D., Lin, B.J., Wang, Y., Li, Y.H., Xu, J.Y., Lin, Y.L., Li, S.H., Lee, Z.J. and Chen, Y.Z., 2023. Building Carbon Emissions Prediction Based on Deep Learning Network with Improved Particle Swarm Optimization. Artificial Intelligence Evolution, pp.216-225.
[11] Ye, L., Du, P. and Wang, S., 2024. Industrial carbon emission forecasting considering external factors based on linear and machine learning models. Journal of Cleaner Production, 434, p.140010.
[12] Kong, D., Dai, Z., Tang, J. and Zhang, H., 2023. Forecasting urban carbon emissions using an Adaboost-STIRPAT model. Frontiers in Environmental Science.
[13] Luo, C., Gao, Y., Jiang, Y., Zhao, C. and Ge, H., 2024. Predictive modeling of carbon emissions in Jiangsu Province's construction industry: An MEA-BP approach. Journal of Building Engineering, p.108903.
[14] Wan, Q. and Liu, J., 2023. Energy efficiency optimization and carbon emission reduction targets of resource-based cities based on BiLSTM-CNN-GAN model. Frontiers in Ecology and Evolution, 11, p.1248426.
[15] Luo, J., Zhuo, W., Liu, S. and Xu, B., 2024. The optimization of carbon emission prediction in low carbon energy economy under big data. IEEE Access.
[16] Ding, Q., Xiao, X. and Kong, D., 2023. Estimating energy-related CO2 emissions using a novel multivariable fuzzy grey model with time-delay and interaction effect characteristics. Energy, 263, p.126005.
[17] Dattatraya, K.N. and Rao, K.R., 2022. Hybrid based cluster head selection for maximizing network lifetime and energy efficiency in WSN. Journal of King Saud University-Computer and Information Sciences, 34(3), pp.716-726.
[18] Gayathri, N., Helen, M. and Mounika, P., 2020. Utilization of Jaccard Index Measures on Multiple Attribute Group Decision Making under Neutrosophic Environment. International Journal of Neutrosophic Science (IJNS), 3(2), pp.67-77.

Doi: https://doi.org/10.54216/IJNS.240127
Received: February 25, 2024 Revised: March 13, 2024 Accepted: April 02, 2024